

Enhancing the memory window of AZO/ZnO/ITO transparent resistive switching devices by modulating the oxygen vacancy concentration of the top electrode

Firman Mangasa Simanjuntak¹ · Debashis Panda² · Tsung-Ling Tsai³ · Chun-An Lin³ · Kung-Hwa Wei¹ · Tseung-Yuen Tseng³

Received: 4 February 2015 / Accepted: 8 July 2015 / Published online: 14 July 2015
© Springer Science+Business Media New York 2015

Abstract The effect of a defect concentration-modified top electrode on the bipolar resistance switching of transparent Al-doped ZnO/ZnO/ITO [AZO(TE)/ZnO/ITO(BE)] devices was investigated. Different oxygen vacancy concentrations in the top electrode, Al-doped ZnO, can be simply controlled by modulating the sputtering working pressure condition from 1.2 to 12 mTorr. The oxygen vacancy concentration between AZO and ZnO may trigger oxygen diffusion at the interface and affect the switching characteristic. High oxygen release from a ZnO resistive layer caused by excessive oxygen vacancy concentration at the top electrode is responsible for reducing the memory window as a result of reduced oxygen available to rupture the filament. Top electrode based on lower oxygen vacancy concentration has a higher memory window and an asymmetric resistive switching characteristic. However, all set of devices have excellent endurance of more than 10^4 cycles. This study showed that an Al-doped ZnO top electrode helps not only to achieve a transparent device but also to enhance memory properties by providing a suitable oxygen vacancy concentration.

Introduction

In recent years, transparent resistive random access memory (T-RRAM) devices have attracted renewed interest because of their potential integration in transparent electronic applications. The use of transparent conducting oxide (TCO) as an electrode satisfies the transparency requirement that metal does not. Low-cost and environmentally friendly Al_2O_3 -doped zinc oxide (AZO) has been investigated for several decades as a potential candidate to substitute high-cost and toxic indium- or tin-based TCO [1]. Nevertheless, for resistive random access memory (RRAM) applications, using transparent AZO as a top electrode is limited. Several studies have been conducted on the influence of different metal electrodes on the characteristics of ZnO-based RRAM [2–6]. However, few studies have investigated the influence of oxide electrodes on the T-RRAM characteristic.

Obtaining favorable endurance properties is one of the major challenges for ZnO-based T-RRAM [7–10]. It has been suggested that the memory window should achieve the requirement of at least one order of magnitude to allow for small and highly efficient sense amplifiers [11, 12]. It has been reported that ITO/ZnO:Mg/FTO exhibits long endurance [13]; however, it lacks an adequate memory window and requires substantial current compliance because of the presence of abundant defects in the switching layer caused by dopant introduction. Therefore, an extremely high current compliance is necessary to provide a suitable memory window. Conversely, some studies have shown a favorable memory window but a lack of endurance [14–18]. This lack of endurance is likely due to insufficient oxygen at the electrode/switching layer interface for preserving long switching. In this study, we achieved excellent endurance for more than 10^4 cycles with

✉ Tseung-Yuen Tseng
tseng@cc.nctu.edu.tw

¹ Department of Materials Science and Engineering, National Chiao Tung University, Hsinchu 30010, Taiwan
² Department of Electronics Engineering, National Institute of Science and Technology, Berhampur 761008, Odisha, India
³ Department of Electronics Engineering and Institute of Electronics, National Chiao Tung University, Hsinchu 30010, Taiwan

a favorable memory window in AZO/ZnO/ITO T-RRAM by merely modifying the oxygen concentration in the AZO top electrode.

Materials and methods

In this study, 50-nm-thick ZnO thin films were deposited on a 320-nm commercial ITO/glass substrate (Merck Display Technologies Ltd, Taoyuan, Taiwan) at room temperature through radio frequency (RF) magnetron sputtering with a ZnO target. The working pressure, power, and Ar/O₂ gas flow were 10 mTorr, 50 W, and 20/10 sccm, respectively. To fabricate a sandwich structure, Al₂O₃-doped ZnO (AZO), which was 150 μm in diameter, was patterned on ZnO/ITO/glass using a metal shadow mask at room temperature at working pressures of 1.2, 2.4, 6, and 12 mTorr. Devices were denoted as *x*AZO, where *x* was 1.2, 2.4, 6, and 12, corresponding to the AZO working pressure condition. A 2 wt% Al₂O₃-doped ZnO target was used to fabricate the top electrode. The thicknesses of the deposited 1.2, 2.4, 6, and 12 mTorr AZO on ZnO/ITO were approximately 541, 514, 464, and 338 nm, respectively. AZO, deposited on a glass substrate, was also prepared to measure the conductivity of AZO films. Transmittance spectroscopy was performed on the devices using a spectrophotometer (U-3010, Hitachi High-Technologies Corp., Tokyo, Japan). The resistive switching characteristic of the devices was measured using a B1500A semiconductor device analyzer (Agilent Technologies, Inc., CA, USA). The crystal structure of the films was studied using an X-ray diffractometer (D8, Bruker Corp., MA, USA). Elemental diffusion was tracked using transmission electron microscopy/energy-dispersive X-ray spectroscopy (TEM/EDS, JEOL 2100FX). The characteristics of oxygen defects in the films were investigated using X-ray photoelectron spectroscopy (XPS) with an etched surface of 30 s (1 Å/s). Binding energy was calibrated using a C1s signal as a reference (with a binding energy of 285.0 eV). Sheet resistance measurement of the AZO films was performed using a HL55WIN Hall system with van der Pauw geometry.

Results and discussion

The T-RRAM devices exhibited high optical transmission (approximately 80 % transmittance in the visible region), as shown in Fig. 1. Such high transmittance indicated that the devices were appropriate for application in transparent memory devices. The thickness and reflection at the interface were responsible for interference fringes that

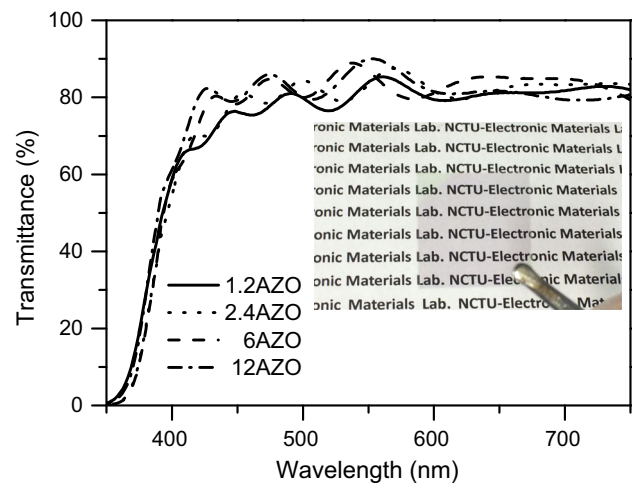


Fig. 1 UV-Vis spectra of the *x*AZO structure. The term *x* corresponds to 1.2, 2.4, 6, and 12 mTorr working pressure conditions (Color figure online)

were observed in transmission spectra [19]. The resistive switching behaviors of the devices were measured by applying a bias voltage at the top electrode while the bottom electrode was grounded. A current compliance of 10 mA was required to avoid permanent breakdown. The devices exhibited a counter-clockwise bipolar switching characteristic, as shown in Fig. 2. A forming process was necessary to switch the devices to a low resistance state (LRS) with a forming voltage of approximately 4.5 V for the 1.2AZO and 2.4AZO devices, and approximately 3.5 V for the 6AZO and 12AZO devices. The devices were switched back to a high resistance state (HRS) by applying a negative bias of -2 V. This process is called the RESET process. The devices were switched back to the LRS again by applying a positive bias of 1.7 V, known as the SET process. Subsequently, switching cycles were conducted by following the same reset and set sequence.

A DC endurance test was conducted to investigate the reliability of the memory devices. The insets of Fig. 2 show the endurance of each device. All the devices were successfully switched for more than 10^4 cycles without any presence of an intermediate state. Devices with AZO fabricated with an increased working pressure showed a tendency to increase the memory window (ON/OFF ratio). The mechanism of resistive switching in metal oxide RRAM is attributable to the generation and recovery of an oxygen vacancy conducting filament with nonlattice oxygen ions [8, 20–22]. Consequently, the phenomena observed in the proposed devices may be related to differences in the amount of available oxygen ions at the interface to reset the device; this was altered using various types of stoichiometric AZO. Therefore, material analyses were conducted in this study to elucidate this phenomenon.

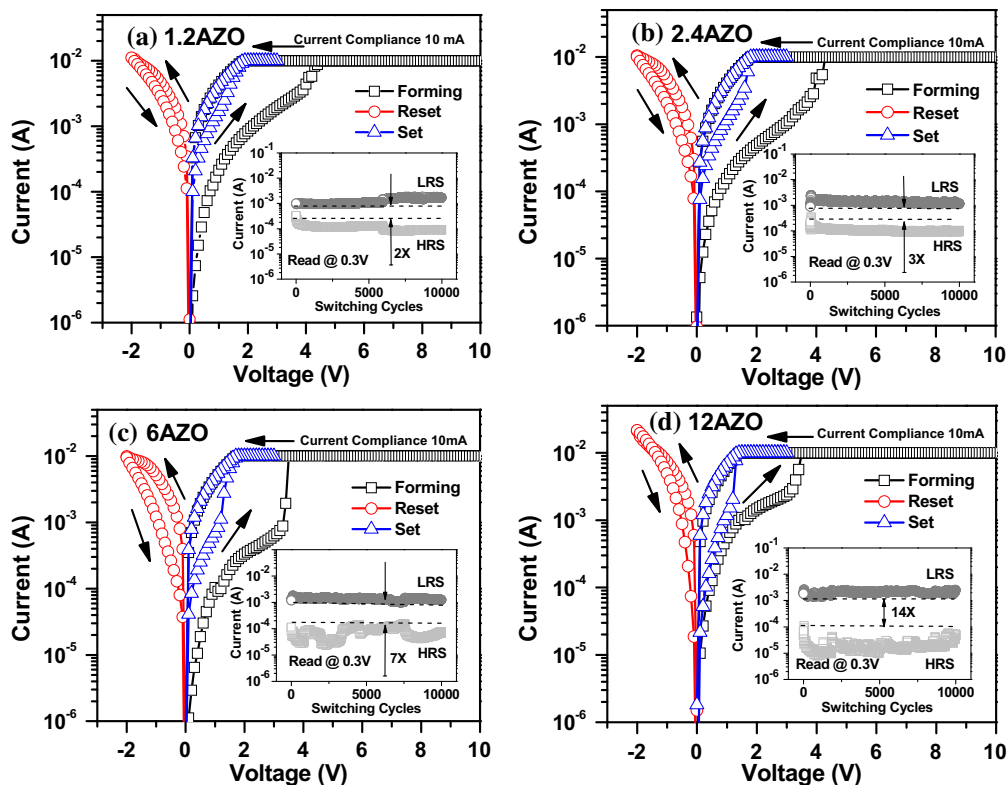


Fig. 2 Switching characteristics of the *I*–*V* curve of the *x*AZO devices. The *inset* shows the endurance performance of the *x*AZO devices (Color figure online)

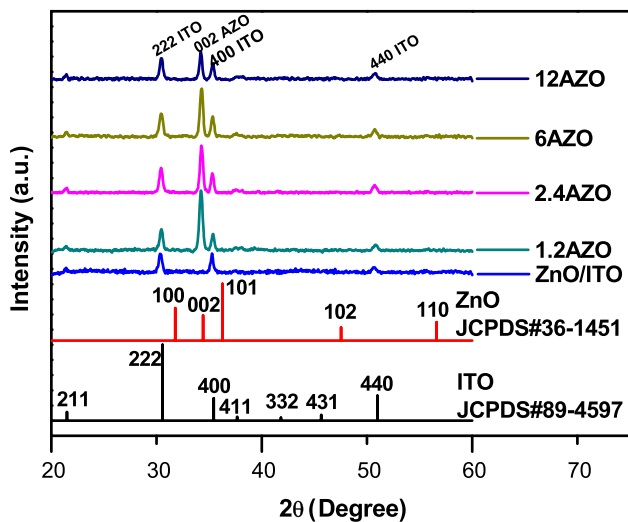


Fig. 3 X-ray diffraction pattern of the *x*AZO structure (Color figure online)

The XRD patterns of the multilayer film structure were investigated to examine their crystal structure, and the results are shown in Fig. 3. Peaks at 30.5°, 35.4°, and 50.9° indicate a cubic ITO structure, whereas the ZnO layer is amorphous because no major peak was detected in the

Table 1 Crystallite size of AZO deposited onto ZnO/ITO

Sample code	FWHM (°)	2θ (°)	Crystallite size (nm)
1.2AZO	0.3633	34.224	23.9116
2.4AZO	0.34975	34.274	24.8471
6AZO	0.36033	34.262	24.1089
12AZO	0.29145	34.207	29.9019

XRD pattern. A strong $\langle 002 \rangle$ peak at 2θ of approximately 34.2° was observed as the wurtzite structure for AZO and no second phase was observed in AZO. The result shows that neither major phase changes nor peak orientation changes are exhibited in AZO by the different working pressures. Crystallite size can be used to reflect the crystallinity of AZO, which can be calculated using the Scherrer formula [23]. AZO fabricated with a higher working pressure tends to have improved crystallinity, as shown in Table 1. The XRD result is consistent with those of previous AZO studies [24, 25]. In addition, AZO stoichiometry has been reported to be strongly correlated with the concentration of oxygen vacancy and can be controlled using the sputtering working pressure condition [24]. Therefore, XPS was conducted to elucidate oxygen-related defects.

Figure 4a shows the XPS spectra of the Zn $2p^{3/2}$ core level of AZO fabricated using various working pressures; Zn $2p^{3/2}$ remains at 1022.4 eV and no metallic Zn is observed with a binding energy of 1021.5 eV, indicating that Zn exists only in the oxidized state [26]. Figure 4b shows the atomic ratios of Al, Zn, and O elements, as well as the oxygen concentration ratio of AZO fabricated using various working pressures. The oxygen concentration ratio increases as the working pressure increases. XPS spectra of the O1s core level of the ZnO and AZO films are shown in Fig. 4c, d, respectively. The spectra were fitted using three nearly Gaussian-resolved peaks. The high binding energy spectrum (Oiii) at 532.4 ± 0.15 eV is attributable to loosely bound chemisorbed oxygen, such as $-\text{CO}_3$, adsorbed H_2O , and O_2 , whereas a medium binding energy (Oii) at 531.25 ± 0.20 eV and low binding energy (Oi) at 530 ± 0.15 eV are, respectively, attributable to the concentration of O^{2-} ions in the oxygen-deficient regions within the ZnO matrix and O^{2-} ions on the wurtzite structure of hexagonal Zn^{2+} ion array surrounded by Zn (or substituted Al) atoms with a full complement of nearest neighbor O^{2-} ions [26].

The changes in the area of Oi and Oii are known to be strongly correlated with the concentration of oxygen vacancies. Figure 4d shows that the area of Oii was substantially larger than Oi, indicating that a large amount of oxygen vacancies existed in the AZO film. An increase of the Oi area at a higher working pressure is attributable to an

increase of the Zn–O bond and a reduction of oxygen vacancies [24]. This tendency was demonstrated in the area ratio of Oii/Oi, which decreased with increasing working pressure, as shown in Fig. 4e. In addition, reducing the oxygen vacancy concentration may cause a downward shift of the Fermi level, and, consequently, an increase in work function [27]. Hence, a higher work function value of AZO fabricated using a higher pressure may lead to a higher leakage current during the forming process.

The AZO electrode fabricated using a lower working pressure had a higher oxygen vacancy concentration compared with the AZO fabricated using a higher working pressure. In addition, the decreasing oxygen vacancy in AZO fabricated using a higher pressure condition increased the sheet resistance of AZO, as shown in Table 2. The XPS and sheet resistance results are consistent with those in previous AZO reports [24, 25]. Conversely, the XPS result of the O1s core level for ZnO showed that Oi was dominant, as shown in Fig. 4c.

Based on the aforementioned analysis, AZO lattices are highly oxygen-deficient compared with ZnO. These two oxygen levels may cause AZO to act as an active material that has the tendency to attract available oxygen from its surroundings. To determine the possible element diffusion between these two films, TEM/EDS observations were conducted. Figure 5a, b shows the TEM image of 2.4AZO/ZnO/ITO and EDS line scanning results, respectively. The EDS spectrum confirmed that an increasing amount of

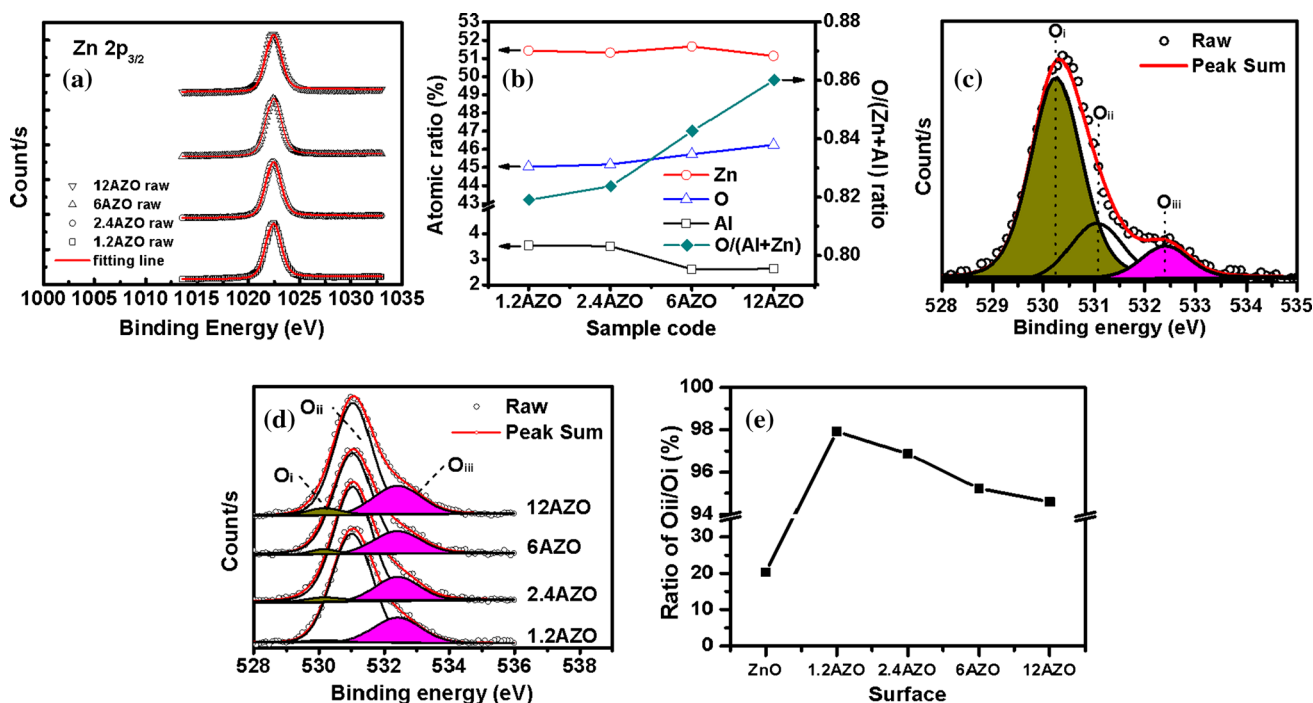
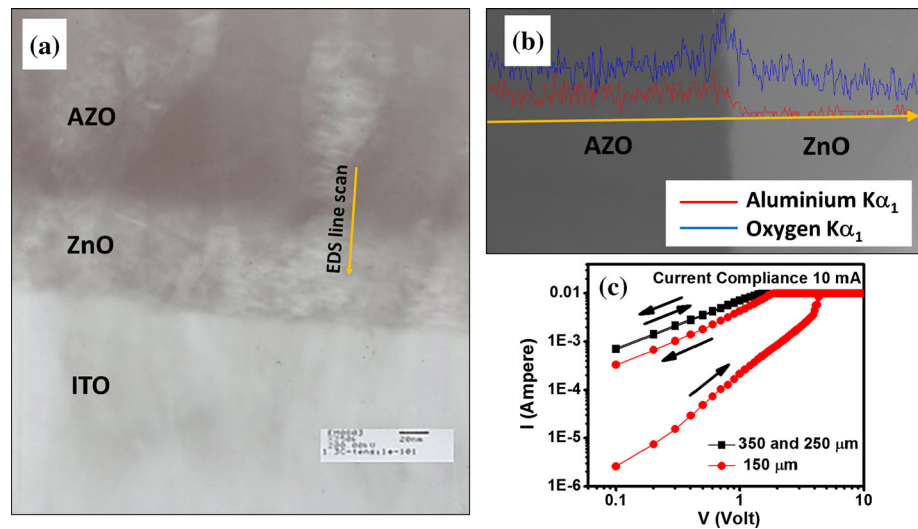


Fig. 4 XPS profile fitting of the Zn $2p^{3/2}$ peak of AZO (a) and the atomic concentration ratio of the elements depending on the working pressure (b), XPS profile fitting of the O1s peak of (c) the ZnO film, (d) AZO film, and (e) ratio of Oii/Oi (Color figure online)

Table 2 Thickness, sheet resistance, and resistivity value of AZO deposited on a glass substrate and ITO/glass

Sample code	Thickness (nm)	Sheet resistance (Ω/\square)	Resistivity ($\times 10^{-3} \Omega \text{ cm}$)
1.2AZO/glass	541	70.42	3.813
2.4AZO/glass	514	133.9	6.889
6AZO/glass	464	317.5	14.75
12AZO/glass	338	505	17.096
ITO/glass	320	15	0.48

Fig. 5 **a** TEM image of the 2.4AZO/ZnO/ITO structure, **b** EDS line scan of **a**, and **c** the log–log plot of the I – V sweep of the pristine 1.2AZO device with a top electrode diameter of 150, 250, and 350 μm (Color figure online)

oxygen accumulated at the AZO/ZnO interface, indicating an oxygen-rich layer. Similar oxygen diffusion toward the top electrode after deposition has also been observed in devices with a metal top electrode [28]. This diffusion may have been detected because of the oxygen vacancy concentration gradient between the two films. A higher concentration of oxygen vacancy in AZO fabricated using a lower pressure resulted in more oxygen being withdrawn from ZnO. Therefore, the increased oxygen deficiency in ZnO increased the conductivity of the ZnO film.

To confirm the oxygen withdrawing phenomena in ZnO, current–voltage (I – V) sweeps on a pristine device with different top electrode sizes were investigated. Figure 5c shows a log–log plot of the first I – V sweep of a pristine 1.2AZO device with top electrode diameters of 150, 250, and 350 μm . No initial resistance state was observed for 1.2AZO devices fabricated with larger electrodes, which may have withdrawn more oxygen from the resistive layer; consequently, the oxygen vacancy defect concentration below the electrode was increased and high leakage was observed.

Statistical analysis was used to elucidate the trend of the memory window [29]. Figure 6a shows the cumulative probability plots of the HRS distribution. The statistical distributions demonstrate that the HRS resistance increased as the oxygen vacancy concentration of the top electrode

decreased. Figure 6b shows the cumulative probability plots of set voltage (V_{set}) distribution. The range of the V_{set} of all devices was within 1.2–1.9 V, which indicates minor dependency of V_{set} on different top electrodes. However, the statistical dispersion may represent the relationship between switching parameters [30, 31]. Figure 6c shows the coefficient of variation (σ/μ) (where σ is the standard deviation and μ is the mean value) of V_{set} and HRS distributions. The lower value of σ/μ means a narrower distribution of the parameter [29]. The results showed that the V_{set} distribution becomes narrower when the HRS distribution is tighter. The statistical analysis indicated that devices fabricated using a higher pressure top electrode tend to have a wider distribution. This phenomenon may be caused by a higher surface roughness at the AZO/ZnO interface because of the high sputtering power.

The dispersion of switching parameters on the V_{set} and R_{off} was dependent on the damage at the top electrode/resistive layer interface [32]. Under high sputtering power condition, a larger voltage drop is present across the plasma and substrate, resulting in more ionized species bombard the growing surface, thus causing more damage to the growing surface and also increasing the surface roughness of the resistive layer [32]. Nevertheless, devices fabricated with a lower pressure top electrode exhibited a narrow V_{set} and HRS dispersion, possibly because of the

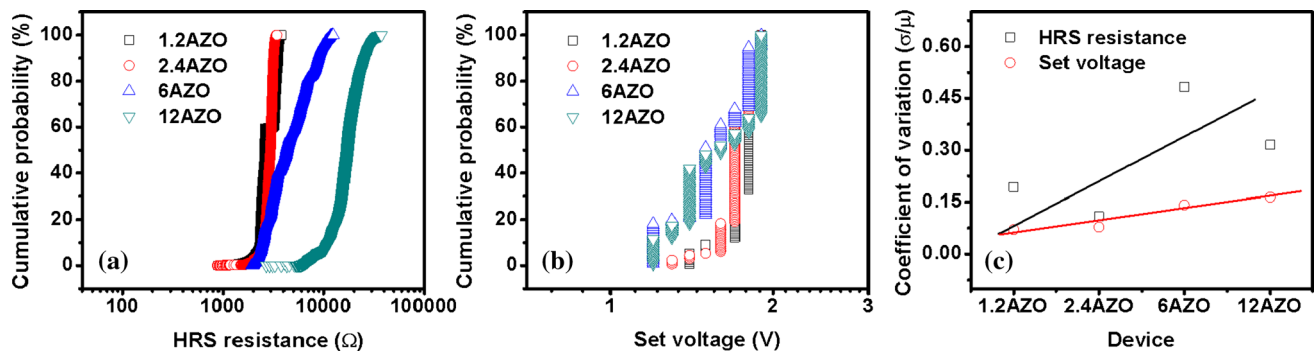


Fig. 6 Cumulative probability plots of **a** the HRS, **b** V_{set} distribution, and **c** coefficient of variation (σ/μ) of (a, b) (Color figure online)

Table 3 Transmittance and memory properties of various ZnO-based T-RRAMs

Structure	Transmittance (in visible region) (%)	Current compliance (mA)	Memory window (times)	Endurance (cycles)
ITO/ZnO/ITO [14]	81	15	$\sim 10^2$	10^2
ITO/ZnO:Mg/FTO [13]	80	50	2.5	10^5
ITO/IGZO/ITO [15]	70–80	10	32	10^2
GZO/ZnO/GZO [7]	~ 80	10	~ 5	7
ITO/GZO/ITO [16]	~ 86.5	0.1	15	350
AZO/MZO/AZO [8]	64–82	1	3	50
GZO/Ga ₂ O ₃ /ZnO/Ga ₂ O ₃ /GZO [17]	92	20	10^2	50
ITO/AZO/ITO [9]	~ 81	10	3	300
ITO/graphene/ZnO/ITO [18]	75.6	5	20	10^2
AZO/ZnO/ITO (this work/12AZO)	~ 80	10	14	10^4

thicker oxygen-rich layer at the interface, which minimized the effect of surface damage. However, further investigation is required to examine this phenomenon. Although devices fabricated with a higher pressure top electrode have a wider distribution, both the HRS and LRS can be obviously distinguished because of the high memory window; furthermore, no intermediate state is exhibited during the 10^4 switching cycles, which can avoid the data read error in RRAM operation.

Long endurance performance (10^4 in Table 3) in the AZO/ZnO/ITO device was achieved because of the existence of an oxygen-rich AZO/ZnO interface layer as the ion-blocking layer, which prevents available oxygen in the resistive layer from diffusing through the grain boundaries of the top electrode and escaping during the set process [28]. Based on the diffusion path, ions more easily diffused through oxide electrode grain boundaries compared with metal electrodes because the length of oxide electrode grain boundaries was substantially shorter than that of metal. Therefore, the ion-blocking layer was necessary for RRAM with a TCO top electrode to preserve oxygen within the resistive layer.

During the positive forming and set process, the ionized oxygen moved toward the ion-blocking layer and then

became interstitial at the interface. Conversely, during the negative reset process, the oxygen was reduced and returned to its vacancy for oxidization; hence, the oxygen vacancy filament was ruptured [8]. The amount of available oxygen to rupture the filament determined the ON/OFF ratio. Therefore, the AZO fabricated using a low pressure exhibited a low ON/OFF ratio because a substantial amount of oxygen from ZnO was initially attracted to the interface to form an oxygen-rich layer.

Table 3 shows the transmittance and memory properties of various ZnO-based resistive switching memories, which indicate that previous studies may have achieved a high memory window but little endurance compared with our report [14–18]; conversely, some previous reports may have achieved long endurance but lacked an adequate memory window [13]. Our memory device has a favorable combination of a moderate current compliance and low applied voltage and a favorable memory window with excellent endurance.

The conduction mechanism of the T-RRAM devices was investigated by plotting I - V curves of the set process region by using a log–log scale and linear fitting. No significant slope differences were observed between the 1.2AZO and 2.4AZO devices, as shown in Fig. 7a. In the

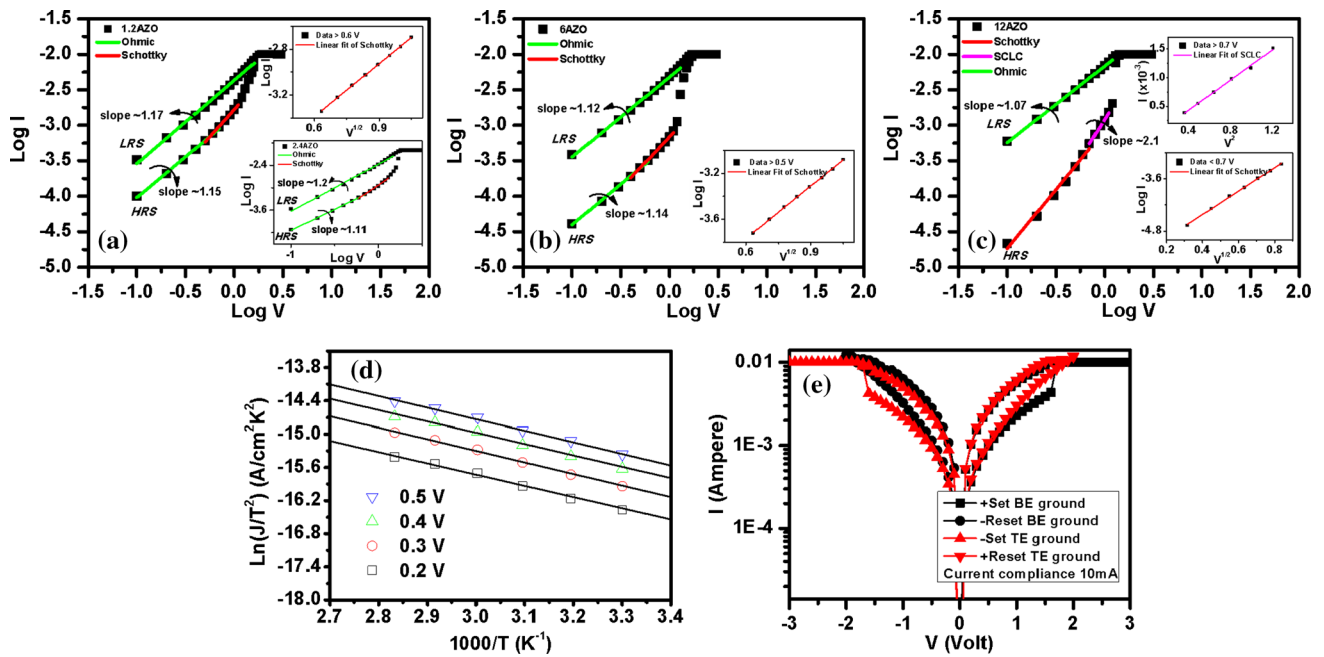


Fig. 7 Log–log plot of the I – V behavior of **a** the 1.2AZO, **b** 6AZO, and **c** 12AZO devices in the SET process region. **d** Temperature-dependent Schottky emission plot of $\text{Ln}(J/T^2)$ vs. $1000/T$ for the 12AZO device, and **e** I – V sweep tests of opposite directions of the

ground on the 12AZO device. The inset shows the log–log plot of the I – V behavior of the 2.4AZO device and the linear fit of Schottky and SCLC emission (Color figure online)

HRS region, Ohmic conduction ($I \propto V$) [33] dominated at the lower voltage region and Schottky conduction ($\log I \propto V^{0.5}$) [33] dominated at the intermediate voltage and then followed by a steep current at higher voltage region right before it switched to the LRS as Ohmic conduction. Similarly, for 6AZO, the HRS was dominated by Ohmic and Schottky conduction at the lower and intermediate voltage region, followed by an abrupt current, as shown in Fig. 7b. In 12AZO, however, Schottky conduction dominated at the lower voltage and was followed by space-charge limited conduction (SCLC, $I \propto V^2$) [34, 35] and an abrupt current at a higher voltage, as shown in Fig. 7c. Figure 7d shows the results of I – V fitting to the Schottky emission conduction measured from 30 to 80 °C for the 12AZO device.

For devices fabricated with a higher pressure top electrode, less oxygen withdrawing would maintain the substantial resistance of the resistive layer. Moreover, a substantial barrier height at the ZnO/ITO interface may have encouraged Schottky emission conduction at the low voltage region. Conversely, the increased withdrawing of oxygen from ZnO caused by AZO fabricated under a lower pressure condition increased the total defect concentration in ZnO and consequently lower the resistance of ZnO. In addition, more oxygen vacancies were generated during forming and resulted in abundant oxygen vacancies accumulated at the ZnO/ITO interface, thus eliminating Schottky emission, and Ohmic emission becomes dominant at the low voltage region. Previous reports have suggested

that reduction and oxidation of ZnO may alter the electron affinity [36, 37]. Reduced ZnO may have increased its electron affinity and promote the elimination of Schottky emission at the ZnO/ITO interface.

An asymmetric I – V curve of the 12AZO device may have occurred because of the modification of the Schottky barrier height at each interface as a result of the differences in the work function between the top and bottom electrodes [38]. A series of I – V sweep tests were conducted to determine whether the work function of electrodes was responsible for the asymmetric behavior and also the existence of the Schottky barrier at the bottom electrode. The test was conducted by changing the directions of ground and DC bias applications, as described in a previous study [16]. As shown in Fig. 7e, the I – V set–reset sweeps of a grounded bottom electrode compared with a grounded top electrode were completely reversed. This result indicated that the work function differences between the ITO bottom electrode and the 12AZO top electrode may have caused the I – V asymmetric curve on this device.

Conclusions

In conclusion, the enhanced memory window and switching behavior of fabricated T-RRAM devices of AZO/ZnO/ITO were investigated. The devices fabricated with a higher pressure top electrode showed a more favorable

memory window because of the appropriate oxygen vacancy concentration of the AZO electrode. Excessive oxygen vacancy concentration at the top electrode may have released more oxygen from the resistive layer, thus reducing the memory window as a result of less oxygen being available to rupture the filament. Nevertheless, the presence of an ion-blocking layer contributed to excellent switching cycle performance in all of the devices. The present study showed that, by using a modest structure and simple fabrication method without dopant introduction to the ZnO resistive layer, favorable endurance can be achieved by merely modifying the AZO top electrode. This study suggests that providing an appropriate oxygen vacancy concentration of the AZO top electrode is also necessary for favorable performance in RRAM.

Acknowledgements This work was supported by the Ministry of Science and Technology, Taiwan, under project NSC 102-2221-E009-134-MY3.

References

- Minami T, Nanto H, Takata S (1984) Highly conductive and transparent aluminium doped zinc oxide thin films prepared by RF magnetron sputtering. *Jpn J Appl Phys* 23:L280–L282. doi:10.1143/JJAP.23.L280
- Tang MH, Jiang B, Xiao YG, Zeng ZQ, Wang ZP, Li JC, He J (2012) Top electrode-dependent resistance switching behaviors of ZnO thin films deposited on Pt/Ti/SiO₂/Si substrate. *Microelectron Eng* 93:35–38. doi:10.1016/j.mee.2011.12.003
- Peng HY, Li GP, Ye JY, Wei ZP, Zhang Z, Wang DD, Xing GZ, Wu T (2010) Electrode dependence of resistive switching in Mn-doped ZnO: filamentary versus interfacial mechanisms. *Appl Phys Lett* 96:192113. doi:10.1063/1.3428365
- Xu D, Xiong Y, Tang M, Zeng B (2013) Top electrode-dependent resistance switching behaviors of lanthanum-doped ZnO film memory devices. *Appl Phys A* 114:1377–1381. doi:10.1007/s00339-013-7994-7
- Chen M-C, Chang T-C, Tsai C-T, Huang S-Y, Chen S-C, Hu C-W, Sze SM, Tsai M-J (2010) Influence of electrode material on the resistive memory switching property of indium gallium zinc oxide thin films. *Appl Phys Lett* 96:262110. doi:10.1063/1.3456379
- Panda D, Tseng T-Y (2013) One-dimensional ZnO nanostructures: fabrication, optoelectronic properties, and device applications. *J Mater Sci* 48:6849–6877. doi:10.1007/s10853-013-7541-0
- Misra P, Das AK, Kukreja LM (2010) Switching characteristics of ZnO based transparent resistive random access memory devices grown by pulsed laser deposition. *Phys Status Solidi* 7:1718–1720. doi:10.1002/pssc.200983244
- Cao X, Li X, Gao X, Liu X, Yang C, Yang R, Jin P (2011) All-ZnO-based transparent resistance random access memory device fully fabricated at room temperature. *J Phys D* 44:255104. doi:10.1088/0022-3727/44/25/255104
- Yu H, Kim M, Kim Y, Lee J, Kim K, Choi S, Cho S (2014) Al-doped ZnO as a switching layer for transparent bipolar resistive switching memory. *Electron Mater Lett* 10:321–324. doi:10.1007/s13391-013-3225-9
- Yao I-C, Lee D-Y, Tseng T-Y, Lin P (2012) Fabrication and resistive switching characteristics of high compact Ga-doped ZnO nanorod thin film devices. *Nanotechnology* 23:145201. doi:10.1088/0957-4484/23/14/145201
- Zhou H, Fang G-J, Zhu Y, Liu N, Li M, Zhao X-Z (2011) Flexible resistive switching memory based on Mn 0.20 Zn 0.80 O/HfO₂ bilayer structure. *J Phys D* 44:445101. doi:10.1088/0022-3727/44/44/445101
- Waser R, Dittmann R, Staikov C, Szot K (2009) Redox-based resistive switching memories nanoionic mechanisms, prospects, and challenges. *Adv Mater* 21:2632–2663. doi:10.1002/adma.200900375
- Shi L, Shang D, Sun J, Shen B (2009) Bipolar resistance switching in fully transparent ZnO:Mg-based devices. *Appl Phys Express* 2:101602. doi:10.1143/APEX.2.101602
- Seo JW, Park J-W, Lim KS, Yang J-H, Kang SJ (2008) Transparent resistive random access memory and its characteristics for nonvolatile resistive switching. *Appl Phys Lett* 93:223505. doi:10.1063/1.3041643
- Chen M-C, Chang T-C, Huang S-Y, Chen S-C, Hu C-W, Tsai C-T, Sze SM (2010) Bipolar resistive switching characteristics of transparent indium gallium zinc oxide resistive random access memory. *Electrochem Solid-State Lett* 13:H191. doi:10.1149/1.3360181
- Kim A, Song K, Kim Y, Moon J (2011) All solution-processed, fully transparent resistive memory devices. *ACS Appl Mater Interfaces* 3:4525–4530. doi:10.1021/am201215e
- Zheng K, Sun XW, Zhao JL, Wang Y, Yu HY, Demir HV, Teo KL (2011) An indium-free transparent resistive switching random access memory. *IEEE Electron Dev Lett* 32:797–799. doi:10.1109/LED.2011.2126017
- Yang P-K, Chang W-Y, Teng P-Y, Jeng S-F, Lin S-J, Chiu P-W, He J-H (2013) Fully transparent resistive memory employing graphene electrodes for eliminating undesired surface effects. *Proc IEEE* 101:1732–1739. doi:10.1109/JPROC.2013.2260112
- Lu JG, Ye ZZ, Zeng YJ, Zhu LP, Wang L, Yuan J, Zhao BH, Liang QL (2006) Structural, optical, and electrical properties of (Zn, Al)O films over a wide range of compositions. *J Appl Phys* 100:073714. doi:10.1063/1.2357638
- Chang W-Y, Lai Y-C, Wu T-B, Wang S-F, Chen F, Tsai M-J (2008) Unipolar resistive switching characteristics of ZnO thin films for nonvolatile memory applications. *Appl Phys Lett* 92:022110. doi:10.1063/1.2834852
- Kwon D-H, Kim KM, Jang JH, Jeon JM, Lee MH, Kim GH, Li X-S, Park G-S, Lee B, Han S, Kim M, Hwang CS (2010) Atomic structure of conducting nanofilaments in TiO₂ resistive switching memory. *Nat Nanotechnol* 5:148–153. doi:10.1038/nnano.2009.456
- Chen JY, Hsin CL, Huang CW, Chiu CH, Huang YT, Lin SJ, Wu WW, Chen LJ (2013) Dynamic evolution of conducting nanofilament in resistive switching memories. *Nano Lett*. doi:10.1021/nl4015638
- Cullity BD, Stock SR (2001) *Elements of X-ray diffraction*. Prentice Hall, Upper Saddle River
- Kim DK, Kim HB (2011) Room temperature deposition of Al-doped ZnO thin films on glass by RF magnetron sputtering under different Ar gas pressure. *J Alloys Compd* 509:421–425. doi:10.1016/j.jallcom.2010.09.047
- Zhang Z, Bao C, Ma S, Zhang L, Hou S (2012) Effects of deposition power and pressure on the crystallinity of Al-doped ZnO thin films at glass substrates by low temperature RF magnetron sputtering. *J Aust Ceram Soc* 48(2):214–222
- Chen M, Wang X, Yu YH, Pei ZL, Bai XD, Sun C, Huang RF, Wen LS (2000) X-ray photoelectron spectroscopy and auger electron spectroscopy studies of Al-doped ZnO films. *Appl Surf Sci* 158:134–140. doi:10.1016/S0169-4332(99)00601-7
- Wang W, Feng Q, Jiang K, Huang J, Zhang X, Song W, Tan R (2011) Dependence of aluminum-doped zinc oxide work function

- on surface cleaning method as studied by ultraviolet and X-ray photoelectron spectroscopies. *Appl Surf Sci* 257:3884–3887. doi:[10.1016/j.apsusc.2010.11.084](https://doi.org/10.1016/j.apsusc.2010.11.084)
28. Young Jeong H, Kyu Kim S, Yong Lee J, Choi S-Y (2011) Role of interface reaction on resistive switching of metal/amorphous TiO₂/Al RRAM devices. *J Electrochem Soc* 158:H979. doi:[10.1149/1.3622295](https://doi.org/10.1149/1.3622295)
29. Wang G, Long S, Yu Z, Zhang M, Li Y, Xu D, Lv H, Liu Q, Yan X, Wang M, Xu X, Liu H, Yang B, Liu M (2015) Impact of program/erase operation on the performances of oxide-based resistive switching memory. *Nanoscale Res Lett*. doi:[10.1186/s11671-014-0721-2](https://doi.org/10.1186/s11671-014-0721-2)
30. Zhang M, Long S, Wang G, Xu X, Li Y, Liu Q, Lv H, Lian X, Miranda E, Suñé J, Liu M (2014) Set statistics in conductive bridge random access memory device with Cu/HfO₂/Pt structure. *Appl Phys Lett* 105:193501. doi:[10.1063/1.4901530](https://doi.org/10.1063/1.4901530)
31. Long S, Lian X, Cagli C, Perniola L, Miranda E, Liu M, Suñé J (2013) A model for the set statistics of RRAM inspired in the percolation model of oxide breakdown. *IEEE Electron Device Lett* 34:999–1001. doi:[10.1109/LED.2013.2266332](https://doi.org/10.1109/LED.2013.2266332)
32. Liu KC, Tzeng WH, Chang KM, Wu CH (2010) The effect of plasma deposition on the electrical characteristics of Pt/HfO_x/TiN RRAM device. *Surf Coat Technol* 205:S379–S384. doi:[10.1016/j.surfcoat.2010.08.043](https://doi.org/10.1016/j.surfcoat.2010.08.043)
33. Gao S, Song C, Chen C, Zeng F, Pan F (2012) Dynamic processes of resistive switching in metallic filament-based organic memory devices. *J Phys Chem C* 116:17955–17959. doi:[10.1021/jp305482c](https://doi.org/10.1021/jp305482c)
34. Pan F, Gao S, Chen C, Song C, Zeng F (2014) Recent progress in resistive random access memories: materials, switching mechanisms, and performance. *Mater Sci Eng R* 83:1–59. doi:[10.1016/j.mser.2014.06.002](https://doi.org/10.1016/j.mser.2014.06.002)
35. Yang YC, Pan F, Liu Q, Liu M, Zeng F (2009) Fully room-temperature-fabricated nonvolatile resistive memory for ultrafast and high-density memory application. *Nano Lett* 9:1636–1643. doi:[10.1021/nl900006g](https://doi.org/10.1021/nl900006g)
36. Jacobi K, Zwicker G, Gutmann A (1984) Work function, electron affinity and band bending of zinc oxide surfaces. *Surf Sci* 141:109–125. doi:[10.1016/0039-6028\(84\)90199-7](https://doi.org/10.1016/0039-6028(84)90199-7)
37. Lee H-Y, Wu B-K, Chern M-Y (2014) Study on the formation of zinc peroxide on zinc oxide with hydrogen peroxide treatment using X-ray photoelectron spectroscopy (XPS). *Electron Mater Lett* 10:51–55. doi:[10.1007/s13391-013-2244-x](https://doi.org/10.1007/s13391-013-2244-x)
38. Kalaev D, Riess I (2013) On conditions leading to crossing of I-V curve in metal1 mixed-ionic–electronic-conductor metal2 devices. *Solid State Ionics* 241:17–24. doi:[10.1016/j.ssi.2013.03.024](https://doi.org/10.1016/j.ssi.2013.03.024)